Triboelectric Nanogenerators as a Self-Powered Motion Tracking System

Mengxiao Chen, Xiaoyi Li, Long Lin, Weiming Du, Xun Han, Jing Zhu, Caofeng Pan, and Zhong Lin Wang**

Motion tracking is a key area of sensor systems for security, transportation, and high-tech industry. In this work, a self-powered motion tracking system is developed to monitor moving speed, direction, acceleration, starting and ending positions, and even the moving path of a moving object. Such a system is based on a set of triboelectric nanogenerators (TENGs) that are composed of two friction layers with opposite triboelectric polarities (Kapton and Aluminum) and operates in the sliding mode. Velocities of a moving object are monitored from −0.1 m s^{-1} to +0.1 m s^{-1} at a step of 0.01 m s^{-1}, and accelerations from −0.1 m s^{-2} to +0.1 m s^{-2} at a step of 0.02 m s^{-2}. Furthermore, an 8 × 8 two-dimensional coordinates system with 16 groups of TENGs is created, and the moving path of an object is obtained. This study opens up a new area of TENGs as active sensors with great potential in self-powered systems, positioning detecting, motion tracking, environmental and infrastructure monitoring, and security.

1. Introduction

Movement tracking system plays an important role in the modern society,[1] such as navigation, aviation, aerospace and defense technology. In the daily life, GPS,[2] speed measuring radar, [3] and wireless locator,[4] which are based on gyroscope,[5] Doppler effect,[6] emission and reception of laser[7] or other signals, are widely used for motion tracking at the large scale. In the meantime, intensive efforts have been made during the last two decades towards the design and development of micro-/nanotechnology for the motion tracking at a small scale. However, powering of these systems still relies on traditional technologies such as batteries. It is highly desirable for motion tracking micro/nanodevices to be self-powered[8] without using a battery in special circumstances of restricted access.[9] Compared to other energy sources like solar energy,[10] chemical energy,[11] water flow and nuclear energy, mechanical energy is one of the most common source of energy in our living environment, especially in a moving system, thus it is the best power source for a self-powered motion tracking device. Diverse approaches have been developed to scavenge mechanical energy based on piezoelectrics,[8,12] electrostatics,[13] and electromagnetics,[14] and so on. Recently, triboelectric nanogenerator (TENG) has been demonstrated as an effective way to convert mechanical energy into electricity.[15] Alternatively, TENG can serve as an active sensor for sensing mechanical vibration/triggering using the electric output by itself without a driving power source.[16] TENGs have been previously demonstrated as a speed sensor of a vehicle[16c] and angular speed sensor.[17]

In this paper, we present a novel self-powered motion tracking system based on TENGs, which are composed of two friction layers with opposite triboelectric polarities[18] (Kapton and Aluminum) and work based on a sliding mode. This tracking system is self-powered and can work without any external power, and it can simultaneously monitor the moving speed, direction, acceleration, starting and ending positions, and even the moving path. Furthermore, we create an 8 × 8 two-dimensional coordinates system with 16 groups of TENGs, and obtain the moving path of an object. This study will open up a new application area of TENGs as active sensors for position detecting, motion tracking, environmental and infrastructure monitoring, and even home security.

2. Results and Discussion

Figure 1 shows the principle and basic structure of a self-powered motion tracking system that is based on a set of sliding mode TENGs.[19] Each TENG has two parts that can slide smoothly with one against the other in contact. One is on the fixed substrate (i.e., road), and the other one is located on the moving object such as an automobile. Thus, signals are generated when the car passes the fixed part of the TENGs (Figure 1a). PMMA was used as a substrate material

M. Chen, X. Li, W. Du, X. Han,
Prof. C. Pan, Prof. Z. L. Wang
Beijing Institute of Nanoenergy and Nanosystems
Chinese Academy of Sciences
Beijing 100083, China
E-mail: cfpan@binn.cas.cn; zlwang@gatech.edu
X. Li, Prof. J. Zhu
Beijing National Center for Electron Microscopy
Department of Material Science and Engineering
Tsinghua University
Beijing 100084, China
L. Lin, Prof. Z. L. Wang
School of Materials Science and Engineering
Georgia Institute of Technology
Atlanta, GA 30332–0245, USA

DOI: 10.1002/adfm.201400431

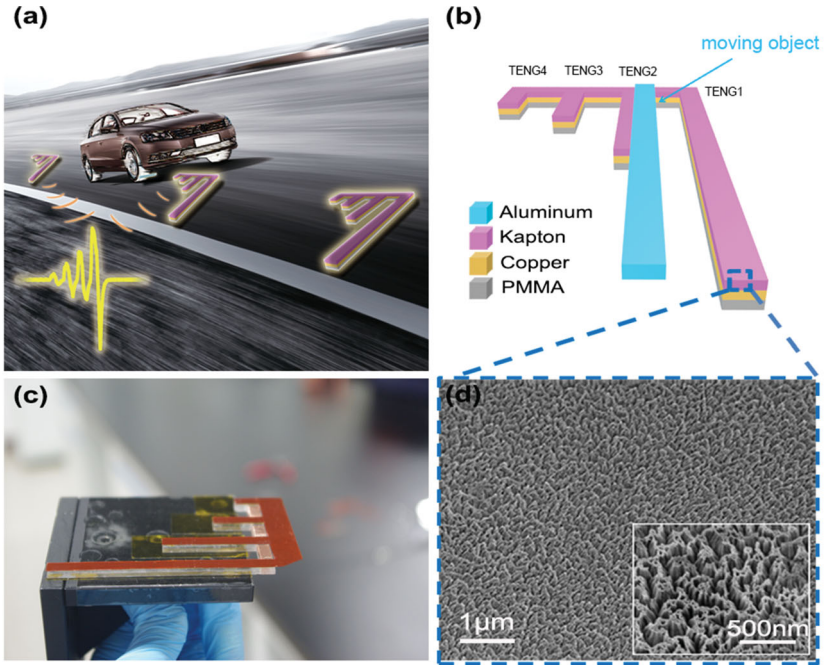

Figure 1. The principle and basic design of a self-powered motion tracking system based on sliding-mode TENGs. a) The principle of a self-powered motion tracking system. Signals are generated when the car passes the TENGs. b) Schematic diagram showing the structural design of the device composing of four TENGs. Each TENG has two parts: one is the fixed substrate (i.e., road), Kapton/PMMA in different sizes coated with copper electrode; and the other one is aluminum covered PMMA located on the moving object like a car. c) A digital image of the as-fabricated device. d) SEM image of the Kapton surface with etched nanowire structure at the tilted view of 30°, the inset is a magnified SEM image.

due to its suitable strength, light weight, easy processing, and low cost. For the upper layer located on the moving object, a layer of aluminum thin foil was covered onto the PMMA substrate, playing dual roles of an electrode and a sliding surface. The four lower layers located on the road were Kapton films of different sizes deposited with Cu electrode (Figure 1c). The detailed fabrication process is discussed in the Experimental Section. To enhance the triboelectrification[20] and increase the effective contact area between the two parts, aligned Kapton nanorod structures could be etched on the Kapton surface by a top-down approach through inductive coupled plasma (ICP) reactive ion etching. A 30 degree-tilted view SEM image of the Kapton NRs is shown in Figure 1d, and a higher magnification SEM image is presented as an insert. It is obvious that the Kapton NRs are uniformly distributed on the Kapton surface with an average diameter of 150 nm and an average length of 600 nm, respectively.

The working principle of the TENGs and the motion tracking system are shown in **Figure 2**. For simplicity, four TENGs with different sizes are illustrated as an example, and the $+x$ axis is set from TENG1 to TENG4. The TENGs are based on the sliding mode triboelectrification. At the original state, the Al and the Kapton films were pre-triboelectrified by sliding with each other. Then the Kapton film was negatively charged, while the copper electrode was positively charged, since Kapton is easier to gain electrons than Al according to the triboelectric series.[21] With the upper moving object (Al film, the blue one) approaching Kapton surface from right-hand side along the $+x$ axis, as shown in Figure 2aI, electrons flow from the Al electrode to the Cu electrode through the external circuit to neutralize the positive triboelectric charges in the Cu electrode, because the Cu electrode beneath the Kapton film has a higher potential than the Al electrode. As a result, a positive signal (noted as I_1) is generated during this process, which is shown in the insert of Figure 2aI. The flow of electrons lasts until the two friction surfaces are fully overlapped, and an electrostatic equilibrium is reached (Figure 2aII). Then the moving object keeps sliding to the left and getting off the Kapton surface, thus the former electrostatic equilibrium is broken (Figure 2aIII). Electrons flow back from the Cu electrode to the Al electrode through the external circuit, generating a negative signal during this process as inserted in Figure 2aIII. Finally, when these two films fully separated with each other again, there is no current flow in the external circuit, and the triboelectric charge distribution returns to the original status (Figure 2aIV). This is a full cycle of the signal generation process. When the upper Al film keeps moving and passing the Kapton films of the other three TENGs, another three current signal peaks (noted as I_2, I_3, I_4) are generated as presented in Figure 2aV–VII. The electron transfer process is similar to the above process described in Figure 2aI to Figure 2aIV. Notably, the absolute output signal value is in proportion to the friction area (here is size of the Kapton films), thus we can find $I_1>I_2>I_3>I_4$ obviously.

For the movement tracking, by measuring the time interval (Δt) between two adjacent peaks, we can get the speed of the moving Al film as $\upsilon = \Delta d/\Delta t$, where Δd is the center-to-center distance between two adjacent TENGs. Acceleration can also be obtained from these measured instantaneous speed values through the υ–t curve. Furthermore, by checking the signal of the output current, we can distinguish whether the moving object moves towards $+x$ direction or $-x$ direction since the output current signal is in proportion to the changing rate of the friction area, relying on which, the movement path of the object can be tracked.

A finite element simulation was carried out to illustrate the electrostatic potential difference when the moving object passed through the first TENG from the right side. The Kapton and aluminum films are closely contact with each other. Friction area here is 5 mm × 80 mm. The Kapton and aluminum are initially assigned with a charge density of -25 μC m^{-2} and 25 μC m^{-2}, respectively, which is the same as the measured value (Figure 2c). The electric potential difference between the two layers at a consecutive sliding displacement of 5 mm can reach 500 V as shown in Figure 2c.

Systematical studies were carried out to explore the speed monitoring using TENG. When the moving object passes

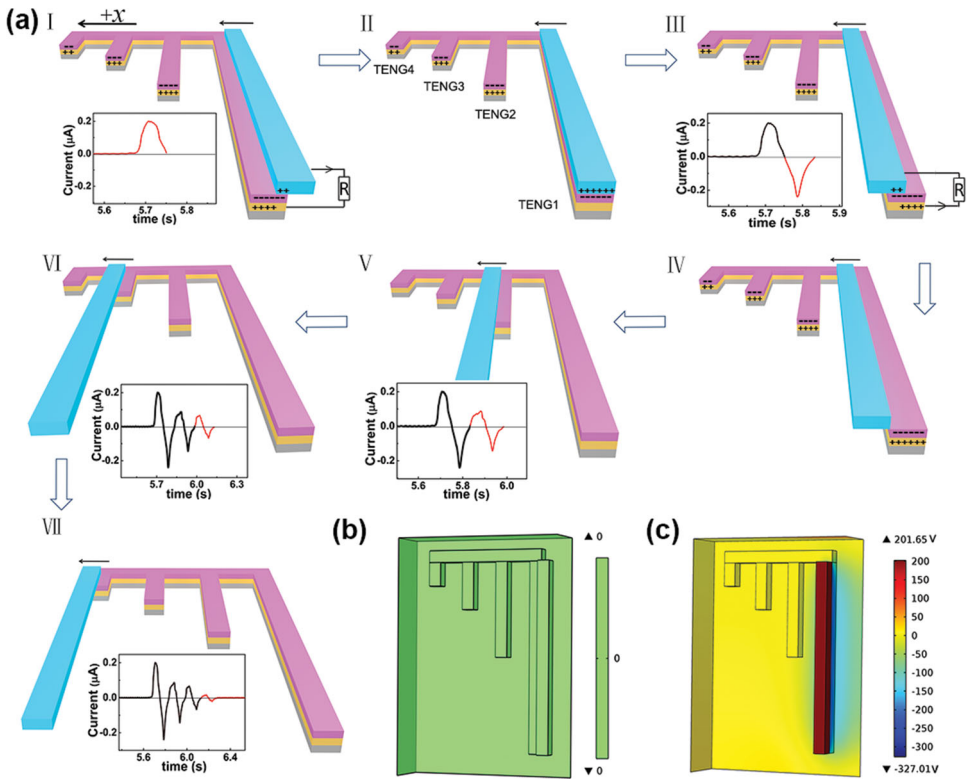

Figure 2. Working mechanism of the TENGs and the motion tracking system. a) The sketches that illustrate a detailed step by step signal generation processes when the moving object passes through the tracking system. (b-c) Finite element simulation of the potential difference between the two electrodes at two different positions: b) 0 mm (the original state) and c) 5 mm (the overlapping position).

TENGs, the self-powered motion tracking system will generate corresponding signal peaks. **Figure 3**a–c are the recorded output signals of voltage, charge quantity, and current when the moving object passed through the four TENGs (from TENG1 to TENG4 and then back to TENG1) with a speed value of 0.1 m/s (Figure 3a). We can obtain the moving speed by any of these three signals. Here, we take the current signal in Figure 3c as an example to extract the speed of the moving object. Speed is the rate at which the displacement of a body changes with time. The center-to-center distance between each two adjacent TENGs is Δd = 15 mm. Assuming that the speed of the moving object was constant during this process, we were able to calculate the instant speed by measuring the time interval of Δt, then the moving speed $\upsilon = \Delta d/\Delta t$. For the one shown in Figure 3c, when the moving object passed through the four TENGs, the time interval measured can be extracted from the recorded signal as Δt_1 = 0.1542 s, Δt_2 = 0.1523 s, Δt_3 = 0.1488 s and Δt_4 = 0.1505 s. Thus, $\upsilon_1 = \Delta d/\Delta t_1$ = 15/0.1542 mm s^{-1} = 0.097 m s^{-1}, $\upsilon_2 = \Delta d/\Delta t_2$ = 15/0.1523 mm s^{-1} = 0.099 m s^{-1}, $\upsilon_3 = \Delta d/\Delta t_3$ = 15/0.1488 mm s^{-1} = 0.101 m s^{-1}, and $\upsilon_4 = \Delta d/\Delta t_4$ = 15/0.1505 mm s^{-1} = 0.100 m s^{-1}. Then, we can get the average measured speed for the moving object as: $\upsilon = (\upsilon_1+\upsilon_2+\upsilon_3+\upsilon_4)/4$ = 0.099 m s^{-1}.

The moving direction is another key element/parameter of a moving object, which can be distinguished by the self-powered motion tracking system as well. Here the speed is regarded as positive when the moving object slides along the +x direction, while the speed is noted as negative when the car slides along the –x direction. It is previously reported that the output current signal of a TENG is in proportion to the changing rate of the friction area.[15b,d] In this work, the friction area of the four TENGs decreases in order, thus the output signal of the four TENGs is $I_1>I_2>I_3>I_4$. For the pink area (left part) of Figures 3a–c, we can conclude that the moving direction is TENG1 to TENG4, since the four signal peaks (any of the current, the voltage, or the charge quantity) decrease in sequence. That is to say, the moving direction is +x direction. While for the yellow area (right part) of Figures 3a–c, we can conclude that the moving direction is reversed, that is, –x direction.

Furthermore, we systematically investigated the response of the self-powered motion tracking system at various moving speeds and directions of the moving object, from –1.0 m/s to 1.0 m/s, with a step of 0.01 m/s. More results are given in Figure S1, Section A in Supporting Information (SI). Figure 3d shows the comparison of the measured speed and actual speed of the moving object. The black points represent the measured moving speeds, and the red line is the actual moving speeds. It is obvious that the measured moving speed and the actual speed fit very well. If the actual moving speed is v_0, the average measured speed is v, we define the speed relative error as: $E_s = (v - v_0)/v_0$. The corresponding actual speed, measured speed, variance of the speed and relative error of each speed are summarized in Table S1, Section A, SI. It can be found that the variance of measured speeds is around 10^{-8}, and most of the errors between the measured and the actual speeds are around 1–2%.

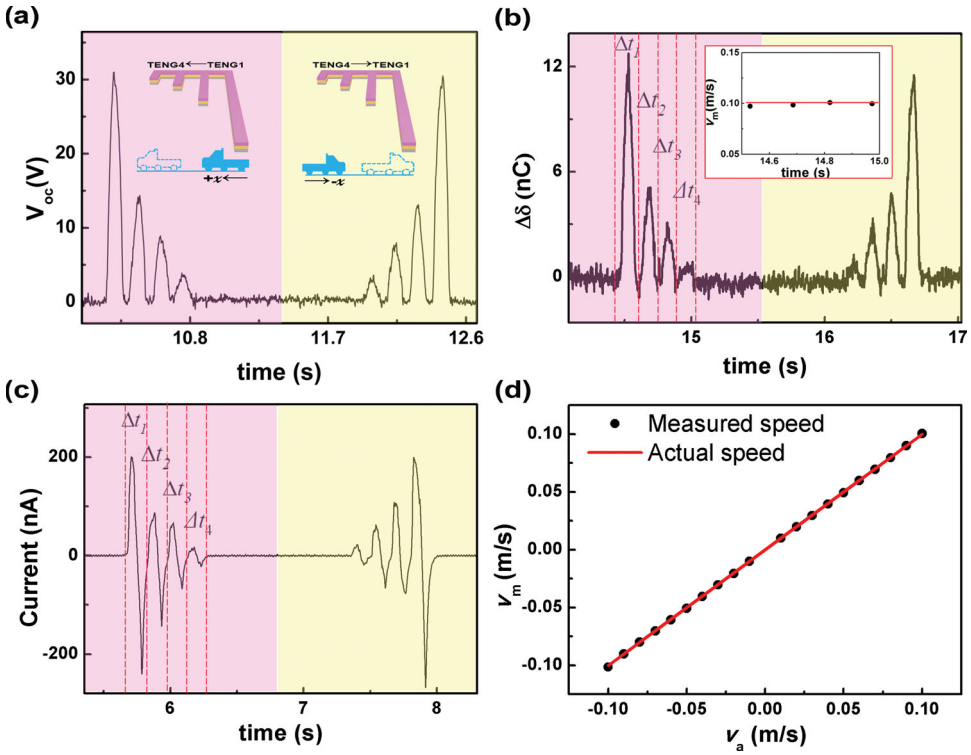

Figure 3. The self-powered motion tracking system serves as a speed sensor. a–c) The output signals of voltage (a), charge quantity (b), and current (c), when the moving object passed through the four TENGs (from TENG1 to TENG 4 and then back to TENG1) with a speed value of 0.1 m s^{-1}. The insert in (a) shows that the object moved from TENG1 to TENG4 at the left part (the pink area), and it moved towards TENG1 at the right part (the yellow area). The speed of the motion could be calculate by measuring the time interval Δt, and then $\upsilon = \Delta d/\Delta t$. (d) The comparison of the measured speed and actual speed of the moving object from –0.1 m s^{-1} to 0.1 m s^{-1} step by 0.01 m s^{-1}, showing a very good consistence with each other.

Figure 4 illustrates that the self-powered motion tracking system serves as an acceleration sensor. Acceleration is the rate at which the velocity of a body changes with time: $a = \frac{\Delta v}{\Delta t}$. As a result, a large number of velocities at different intervals of time or the *v*–*t* curve is required to get the instantaneous acceleration value. For simplicity, we take uniformly accelerated rectilinear motion (its *v*-*t* curve is a straight line) as an example for demonstration how to obtain the acceleration information by the self-powered movement tracking system. In such case, the acceleration over a period of time is the change in velocity divided by the duration of the period $a = \frac{\Delta v}{\Delta t}$, which can also be read out as the slope of the *v*–*t* curve. According to the output current signals in Figure 4a, we can get the absolute value of the speed the same method used in Figure 3: $v_1 = \Delta d/\Delta t_1 = 15/0.3539$ mm s^{-1} = 0.042 m s^{-1} $\Delta v_2 = \Delta d/\Delta t_2 = 15/0.2288$ mm s^{-1} = 0.066 m/s and $v_3 = \Delta d/\Delta t_3 = 15/0.1775$ mm s^{-1} = 0.084 m s^{-1}. The corresponding *v*–*t* curve is presented in Figure 4b, in which the red points represent the measured moving speeds, and the black line is the fitting line. It is obviously that the data linear fits very well and we can get the acceleration by calculating the slope of the *v*–*t* curve, which is about 0.0856 m s^{-2}, quite close to the actual acceleration 0.08 m s^{-2} with an error of 7%. And the acceleration direction can be distinguished by the slope of fitting line. In Figure 4c,d, the measured acceleration for this group of signals is –0.085 m s^{-2}, compared with actual acceleration –0.08 m s^{-2}. Furthermore, we systematically investigated the response of the self-powered motion tracking system at various moving accelerations, from –1.0 m s^{-2} to 1.0 m s^{-2}, with a step of 0.02 m s^{-2}. More results are given in Figure S2, Section B in Supporting Information (SI). Figure 4e shows the comparison of the measured acceleration and actual acceleration of the moving object. The black points represent the measured accelerations, and the red line is the actual accelerations. If the actual acceleration is a_0, the average measured acceleration is *a*, we define the relative deviation of the acceleration as: $E_a = (a - a_0)/a_0$. The corresponding actual acceleration, measured acceleration, variance of the acceleration and relative error of each acceleration are summarized in Table S2, Section B, SI. It can be found that the variance of measured accelerations is around 10^{-6}, and most of the errors between the measured and the actual accelerations range from 1% to 10%.

Last but the most important, the location and moving path are two most important but difficult parameters for tracking an object besides speed, acceleration, and direction. We need to know the accurate coordinates of the starting position (x_1,y_1), ending point (x_2,y_2) and the path of the moving object in a 2-dimensional system. As aforementioned, the output signal of a TENG is in proportion to the changing rate of the friction area. So if an object passes through two TENGs with different friction areas, the TENGs will give two different output signals: the larger one can be treated as signal "1", while the smaller signal can be treated as "0". Thus, four TENGs could work as a 4-bits binary code generator. Inspired by this, we introduce the binary system to build a 2-dimensional (*x*,*y*) coordinates, as

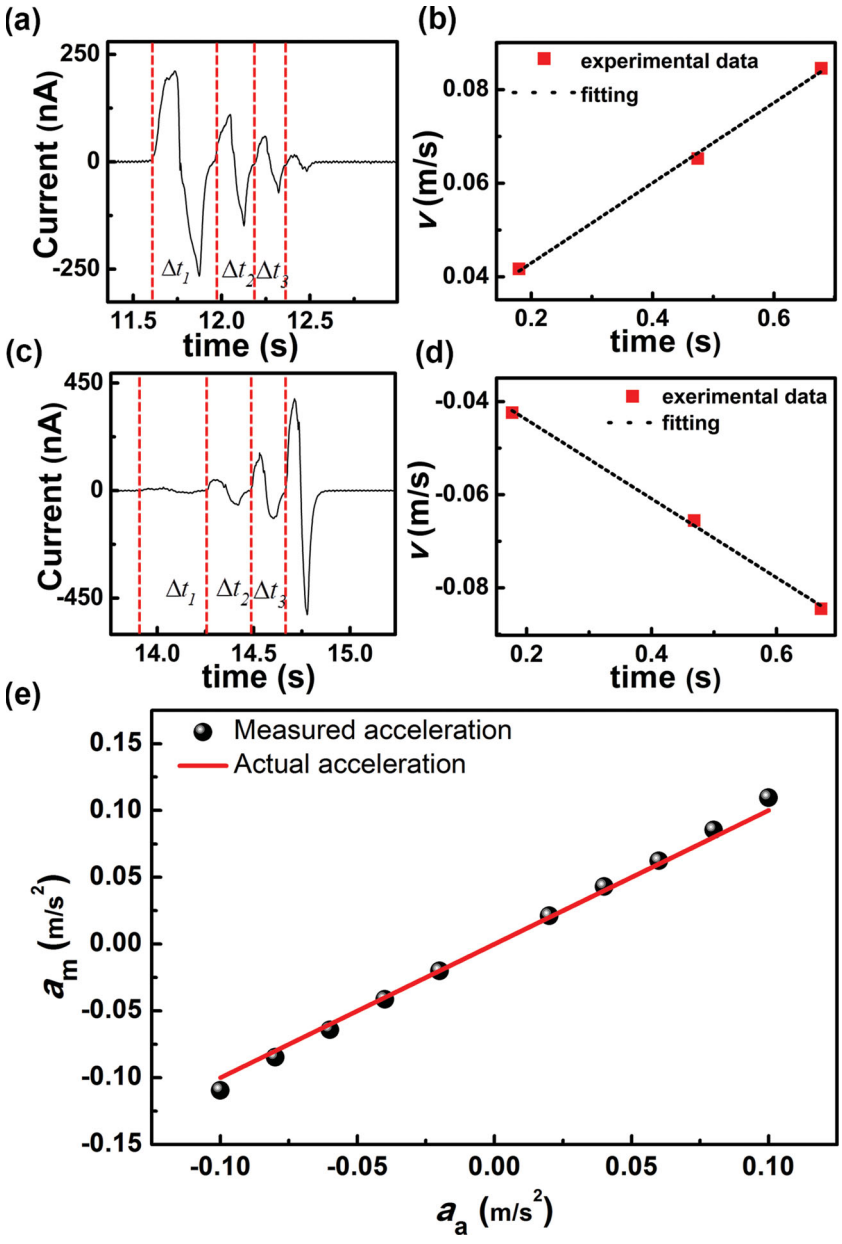

Figure 4. The acceleration monitoring of a moving object by the self-powered motion tracking system. a) The current output signals when the object passed through the four TENGs (from TENG1 to TENG4) in a uniformly accelerated rectilinear motion with an acceleration of +0.08 m s^{-2}. b) Linear fitting of measured speeds which are extracted from Figure 4a with the same method in Figure 3, and the slope of the fitting curve is the measured acceleration. c) The output signals of current when the object passed through the four TENGs (from TENG4 to TENG1) in a uniformly accelerated rectilinear motion with an acceleration of –0.08 m s^{-2}. d) Linear fitting of measured speed, and the slope of the fitting curve is the measured acceleration. e) The comparison of the measured and actual accelerations.

shown in **Figure 5**a. Units composing a group of TENGs with two kinds of different friction area are used. Take a 4-bits unit as an example, "0001" in the binary system stands for "1" in the decimal system, while "0010" in the binary system is "2" in the decimal system. Based on such 4-bits binary system, we create an 8 × 8 2D coordinates system with 16 sets of TENGs. To distinguish whether the object moving along the *x*-axis or the *y*-axis, all the numbers on *x*-axis are odd and all the numbers on *y*-axis are even, as shown in Figure 5a.

Figures 5b,c and 5d,e are two examples that demonstrate how to monitor the moving path when the object moves along the *x*-axis and the *y*-axis, respectively. In Figure 5b, when the object passes the two units, it generates two groups of signals. Each group of signals composes of four peaks, which is presented in Figure 5c. By checking the signals, we can find that the signals generated by the first unit are two low level signals and two high level signals in sequence, marked as "0011" in the binary system, which stands for "3" in the decimal system. The signal generated by the second unit is "0101" in the binary system, which means "5" in the decimal system. As a result, we can conclude that the moving path of this object is along the *x*-axis, from (1,0) to (5,0). Details of the analysis on how to determine the moving path of the object can be found in the Figure S5 Section D, SI. Similarly, in Figures 5d–5e, when the object moved along the two units along the *y*-axis, two groups of signals were generated as "0100" and "0110" in the binary system, which were corresponding to "4" and "6" in the decimal system. Thus we can also conclude that the moving path of this object is along the *y*-axis, from (0,2) to (0,6).

Finally, we present a systematical tracking of an object, including the moving speed, the moving direction, and the path by the self-powered motion tracking system in one step, as shown in Figure 5f. There are 3 moving processes, which are marked as zone (I), zone (II) and zone (III). According to the three sets of signals "1010", "0100", and "1100", we can conclude the moving path of this object is (5,2) → (3,2) →(3,4) →(1,4), as shown in Figure 5a by the green line. The speed during each process can be calculated with the same method in Figure 3, and they are v_I = 0.010 m s^{-1}, v_{II} = 0.016 m s^{-1}, and v_{III} = 0.009 m s^{-1}. The overall moving information of this object is: the object started at (5,2), and moved to (3,2) along the –*x* axis with a velocity of –0.010 m s^{-1}; then it turned right, moved from (3,2) to (3,4) along the +*y*-axis with a velocity of +0.016 m s^{-1}; lastly, it turned left, moved from (3,4) to (1,4) along the –*x* axis with a velocity of –0.009 m s^{-1}.

The self-powered motion tracking system offers a few unique advantages for motion tracking. First, this device can work as an active sensor for tracking motion using the electric output generated by itself without an external power source, since the tracking system is built on TENGs that can convert mechanical energy into electricity. For example, when earthquake happens,

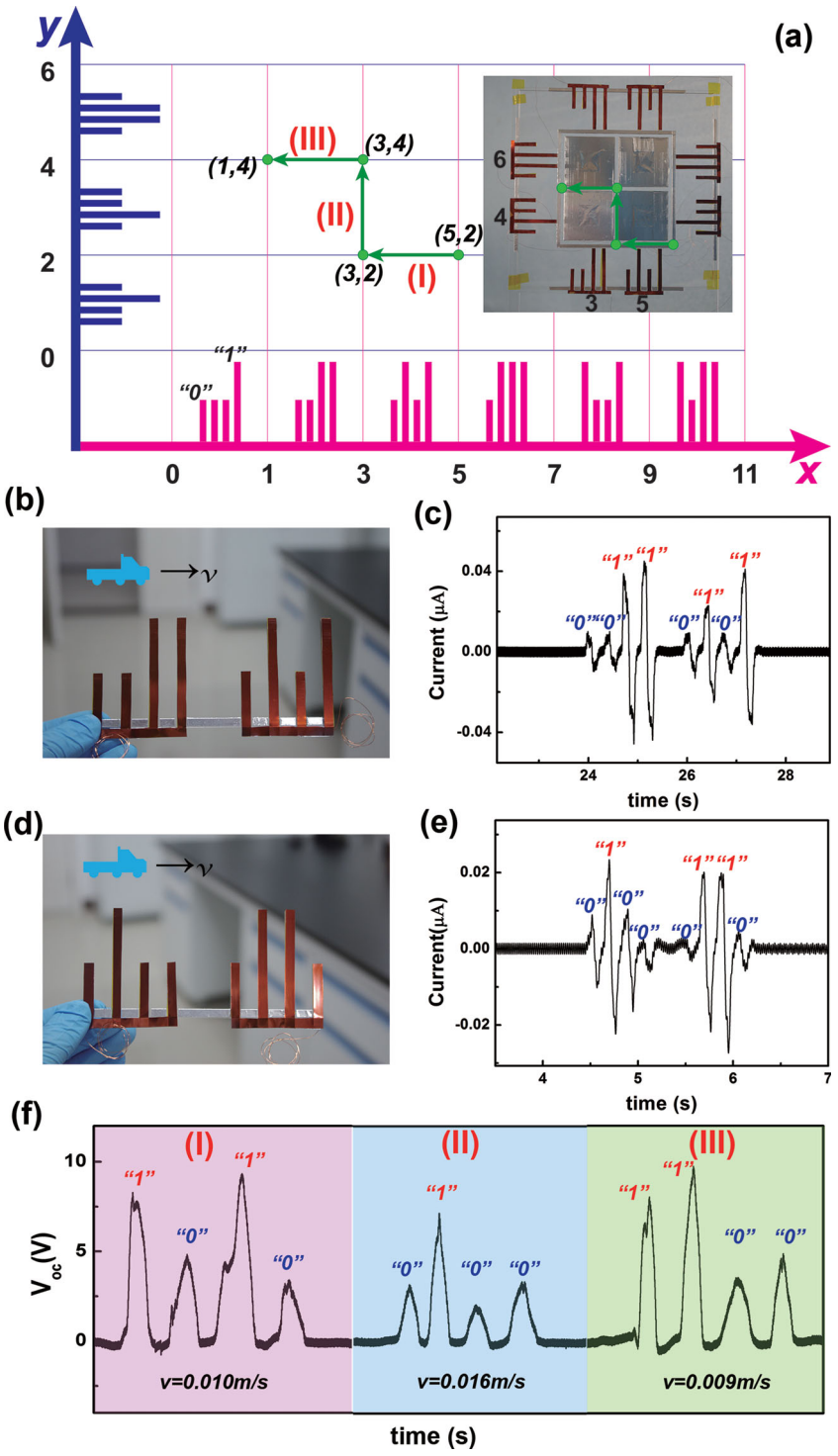

Figure 5. A novel design for the 2-dimension location and moving path monitoring. a) A 2D 8 × 8 (*x*,*y*) coordinates created by 16 groups of TENGs. There are two kinds of TENGs here, a longer one giving a high level signal meaning "1" in the binary system, while a shorter TENG giving a low level signal standing for "0" in the binary system. Thus, each group of TENGs is a 4-bits binary system, which stands for 0 to 15 in the decimal system. Furthermore, all the numbers on *x*-axis are odd and all the numbers on *y*-axis are even. A photograph showing part of such system is presented as the insert. b,c) A digital photograph and the corresponding output signals indicate an object passed through (1,0) to (5,0) along the *x*-axis at a speed of +0.04 m s^{-1}. d,e) A digital photograph and the corresponding output signals indicate an object passed through (0,2) to (0,6) along the *y*-axis at a speed of +0.08 m s^{-1}. f) A systematical tracking of an object, including the moving speed, direction, and the path by the self-powered motion tracking system: the object started at (5,2), and moved to (3,2) along the –*x* axis with a velocity of –0.010 m s^{-1}; then it turned right, moved from (3,2) to (3,4) along the +*y*-axis with a velocity of +0.016 m s^{-1}; lastly, it turned left, moved from (3,4) to (1,4) along the –*x* axis with a velocity of –0.009 m s^{-1}. The final path is (5,2) → (3,2) →(3,4) →(1,4), which is highlighted with green lines in the Figure 5a.

the power supply is usually off. Most electric appliances could not work under this circumstance, however, the proposed TENG based device could work as usual with its self-powered operations. Second, current traffic monitoring technologies are mainly based on optical ways depending on visibility, such as CCDs and so on. However, the traditional CCD could not get specific information on the road when the weather is bad, such as fog, haze, rain, snow and other harsh low visible day. But our TENG based motion tracking device can work very well, since the signal measured is electric signal. Third, although only a 4-bits binary system (8 pixels × 8 pixels) was demonstrated in this work to illustrate the motion path tracking in two dimensions, we can extend this system by increasing the number of bits in each unit; for example, we can get a system with 16 384 pixels by using an 8-bits binary system. Third, this motion tracking system can only monitor the moving parallel to the *x*- or *y*-axis at the current stage; more efforts are required to upgrade this system to track the moving in any direction.

Furthermore, in order to prove that our device could be applicable to measuring real car speed and work normally in some special weather, for example, the rain, in Supporting Information, we provide some videos and further detail discussion to support it. Firstly, we accommodate our device to a model car. After the model working, we made true application on walking monitoring, bicycle monitoring (Figure S6, Video 1, SI), "actual car speed" monitoring (reached 31.82 km h^{-1}, Figure S7, Video 2, SI), vehicle flow monitoring and counting (dry and wet conditions, Video 3 and Video 4).

3. Conclusion

In summary, we demonstrate a novel self-powered motion tracking system based on a set of sliding-mode TENGs, which are composed of two friction layers with opposite triboelectric polarities. It can monitor the moving speed, direction, acceleration, starting and ending positions, and even the moving path. We have demonstrated to monitor the velocities of a moving object like a car varying from –0.1 m s^{-1} to +0.1 m s^{-1} step by 0.01 m s^{-1}, and accelerations from –0.1 m s^{-2} to +0.1 m s^{-2} step by 0.02 m s^{-2}, with an error range of 0.1% to 2.25% and 1.25% to 10%, respectively. Furthermore, we obtain the moving path of an object with two turnings by creating an 8 × 8 2-dimensional coordinates system with 16 sets of TENGs. This study will open up a new area of TENGs with numerous advantages as active sensors, with great potential in self-powered systems, positioning detecting, motion tracking, environmental and infrastructure monitoring, and home security.

4. Experimental Section

Fabrication of the Kapton Nanorods: A 140 μm thick Kapton film was cleaned with menthol, isopropyl alcohol, and deionized water, consecutively, and then blown dry with air. Then, the surface of the Kapton was deposited with a 10 nm Au thin film by sputtering as the mask for the following etching of the Kapton surface to create the nanorod structure using the inductively coupled plasma (ICP) reactive ion etching. Specifically, Ar and O_2 gases were introduced into the ICP chamber with the flow rate of 5.0 and 55.0 sccm, respectively. One power source of 500 W was used to generate a large density of plasma, and the other power of 100 W was used to accelerate the plasma ions. A field emission scanning electron microscopy (FESEM, Hitach S5500) was used to characterize the Kapton NRs after a one-minute ICP etching.

Fabrication of TENGs: First, two 3 mm-thickness and 5 mm-width PMMA sheets were used as substrates. The four lower layers located on the road are Kapton film in different lengths (80 mm, 40 mm, 20 mm, and 10 mm) deposited with Cu electrode. The center-to- center distance between every adjacent TENGs is 15 mm. The other part located on the moving object is a 5 mm × 80 mm PMMA covered with Al thin film.

Fabrication of the Self-Powered Motion Tracking System: Two kinds of the as-prepared TENGs with the friction area of 30 mm × 5 mm and 60 mm × 5 mm were used to generate low level "0" and high level signals "1". Four such TENGs form a unit like a 4-bits binary system. 16 units of TENGs, such as "0001", "0010", "0100", create an 8 × 8 2-dimensional coordinates system. All the odd numbers (like "0001", "0011", "0101", "0111", "1001", "1011" "1101", "1111") are on *x*-axis, while all the even numbers (like "0000", "0010", "0100", "0110", "1000", "1010" "1100", "1110") are on *y*-axis.

Electrical Output Measurement of the Self-Powered Motion Tracking System: In the electrical output measurement, the upper Al part of the TENGs was bonded onto a linear motor (Linmot E1100) like a car, and the Kapton part was secured on a fixed XYZ bearing linear stages (Newport Corporation, M-462-XYZ). The open-circuit voltage and transferred charge quantity was measured by Keithley 6514 electrometer, and the short-circuit current was measured by SR570 low noise current amplifier (Stanford Research System).

Supporting Information

Supporting Information is available from the Wiley Online Library or from the author.

Acknowledgements

M.C. and X.L. contributed equally to this work. The authors thank for the support from the "thousands talents" program for pioneer researcher and his innovation team, China, and the Knowledge Innovation Program of the Chinese Academy of SciencesGrant No. KJCX2-YW-M13).

Received: February 7, 2014
Revised: March 22, 2014
Published online: May 7, 2014

[1] a) C. Vieren, F. Cabestaing, J. G. Postaire, *Pattern Recogn. Lett.* **1995**, *16*, 679; b) F. Gustafsson, F. Gunnarsson, N. Bergman, U. Forssell, J. Jansson, R. Karlsson, P. J. Nordlund, *IEEE Trans. Signal. Proces.* **2002**, *50*, 425; c) O. Julien, C. MacAbiau, M. E. Cannon, G. Lachapelle, *IEEE Trans. Aero. Electron. Syst.* **2007**, *43*, 150.

[2] a) M. Bevis, S. Businger, T. A. Herring, C. Rocken, R. A. Anthes, R. H. Ware, *J. Geophys. Res-Atmos.* **1992**, *97*, 15787; b) W. I. Bertiger, Y. E. Barsever, E. J. Christensen, E. S. Davis, J. R. Guinn, B. J. Haines, R. W. Ibanezmeier, J. R. Jee, S. M. Lichten, W. G. Melbourne, R. J. Muellerschoen, T. N. Munson, Y. Vigue, S. C. Wu, T. P. Yunck, B. E. Schutz, P. A. M. Abusali, H. J. Rim, M. M. Watkins, P. Willis, *J. Geophys. Res-Oceans.* **1994**, *99*, 24449.

[3] P. Bahl, V. N. Padmanabhan, presented at INFOCOM. RADAR: *An in-building RF-based user location and tracking system*, Tel Aviv, Israel **March, 2000**.

[4] A. Tarighat, N. Khajehnouri, A. H. Sayed, presented at ICASP. *Improved Wireless Location Accuracy Using Antenna Arrays and Interference Cancellation*, Hong Kong, China **April, 2003**.

[5] R. E. Mayagoitia, A. V. Nene, P. H. Veltink, *J. Biomech.* **2002**, *35*, 537.
[6] W. Kündig, *Phys. Rev.* **1963**, *129*, 2371.
[7] M. Vincze, J. Prenninger, H. Gander, *Int. J. Robot. Res.* **1994**, *13*, 305.
[8] Z. L. Wang, J. H. Song, *Science* **2006**, *312*, 242.
[9] a) Z. L. Wang, W. Z. Wu, *Angew. Chem. Int. Edit.* **2012**, *51*, 11700; b) Z. L. Wang, *Adv. Mater.* **2012**, *24*, 280; c) Z. L. Wang, *Sci. Am.* **2008**, *298*, 82; d) Z. L. Wang, *Adv. Funct. Mater.* **2008**, *18*, 3553.
[10] a) C. F. Pan, S. M. Niu, Y. Ding, L. Dong, R. M. Yu, Y. Liu, G. Zhu, Z. L. Wang, *Nano Lett.* **2012**, *12*, 3302; b) C. F. Pan, Z. X. Luo, C. Xu, J. Luo, R. R. Liang, G. Zhu, W. Z. Wu, W. X. Guo, X. X. Yan, J. Xu, Z. L. Wang, J. Zhu, *ACS Nano* **2011**, *5*, 6629.
[11] a) C. F. Pan, Y. Fang, H. Wu, M. Ahmad, Z. X. Luo, Q. A. Li, J. B. Xie, X. X. Yan, L. H. Wu, Z. L. Wang, J. Zhu, *Adv. Mater.* **2010**, *22*, 5388; b) C. F. Pan, H. Wu, C. Wang, B. Wang, L. Zhang, Z. D. Cheng, P. Hu, W. Pan, Z. Y. Zhou, X. Yang, J. Zhu, *Adv. Mater.* **2008**, *20*, 1644; c) C. F. Pan, J. Luo, J. Zhu, *Nano Res.* **2011**, *4*, 1099; d) C. F. Pan, Z. T. Li, W. X. Guo, J. Zhu, Z. L. Wang, *Angew. Chem. Int. Ed.* **2011**, *50*, 11192.
[12] a) X. D. Wang, J. H. Song, J. Liu, Z. L. Wang, *Science* **2007**, *316*, 102; b) Y. Qin, X. D. Wang, Z. L. Wang, *Nature* **2008**, *451*, 809.
[13] a) P. D. Mitcheson, P. Miao, B. H. Stark, E. M. Yeatman, A. S. Holmes, T. C. Green, *Sens. Actuators A* **2004**, *115*, 523; b) R. Pelrine, R. Kornbluh, J. Eckerle, P. Jeuck, S. J. Oh, Q. B. Pei, S. Stanford, *S. Proc. SPIE* **2001**, *4329*, 148.
[14] a) T. von Buren, P. D. Mitcheson, T. C. Green, E. M. Yeatman, A. S. Holmes, G. Troster, *IEEE Sens. J.* **2006**, *6*, 28; b) S. P. Beeby, R. N. Torah, M. J. Tudor, P. Glynne-Jones, T. O'Donnell, C. R. Saha, S. Roy, *J. Micromech. Microeng.* **2007**, *17*, 1257.
[15] a) F. R. Fan, Z. Q. Tian, Z. L. Wang, *Nano Energy* **2012**, *1*, 328; b) G. Zhu, Z. H. Lin, Q. S. Jing, P. Bai, C. F. Pan, Y. Yang, Y. S. Zhou, Z. L. Wang, *Nano Lett.* **2013**, *13*, 847; c) G. Zhu, J. Chen, Y. Liu, P. Bai, Y. S. Zhou, Q. S. Jing, C. F. Pan, Z. L. Wang, *Nano Lett.* **2013**, *13*, 2282; d) Y. S. Zhou, Y. Liu, G. Zhu, Z. H. Lin, C. F. Pan, Q. S. Jing, Z. L. Wang, *Nano Lett.* **2013**, *13*, 2771; e) G. Zhu, C. F. Pan, W. X. Guo, C. Y. Chen, Y. S. Zhou, R. M. Yu, Z. L. Wang, *Nano Lett.* **2012**, *12*, 4960.
[16] a) Z. L. Wang, *ACS Nano* **2013**, 9533; b) Y. Yang, H. L. Zhang, J. Chen, Q. S. Jing, Y. S. Zhou, X. N. Wen, Z. L. Wang, *ACS Nano* **2013**, *7*, 7342; c) L. Lin, Y. F. Hu, C. Xu, Y. Zhang, R. Zhang, X. N. Wen, Z. L. Wang, *Nano Energy* **2013**, *2*, 75; d) Y. Hu, J. Yang, Q. Jing, S. Niu, W. Wu, Z. L. Wang, *ACS Nano* **2013**, 10424.
[17] L. Lin, S. H. Wang, Y. N. Xie, Q. S. Jing, S. M. Niu, Y. F. Hu, Z. L. Wang, *Nano Lett.* **2013**, *13*, 2916.
[18] A. F. Diaz, R. M. Felix-Navarro, *J. Electrostat.* **2004**, *62*, 277.
[19] a) S. H. Wang, L. Lin, Y. N. Xie, Q. S. Jing, S. M. Niu, Z. L. Wang, *Nano Lett.* **2013**, *13*, 2226; b) S. Niu, Y. Liu, S. Wang, Long Lin, Y. S. Zhou, Y. Hu, Zhong Lin Wang, *Adv. Mater.* **2013**, *25*, 6184.
[20] G. S. P. Castle, *J. Electrostat.* **1997**, *40–1*, 13.
[21] J. C. Wilcke, *Disputatio Physica Experimentalis, De Electricitatibus Contrariis*, Rostochii: Typis Ioannis Iacobi Adleri, **1757**.